EDGE ARTICLE

Check for updates

Polarization of macrophages to an anti-cancer phenotype through *in situ* uncaging of a TLR 7/8 agonist using bioorthogonal nanozymes†

Xianzhi Zhang, ‡[a] Yuanchang Liu,‡[a] Mingdi Jiang, ‡[a] Javier A. Mas-Rosario,[ab] Stefano Fedeli,[a] Roberto Cao-Milan,[a] Liang Liu,[a] Kyle J. Winters,[a] Cristina-Maria Hirschbiegel,[a] Ahmed Nabawy,[a] Rui Huang,[a] Michelle E. Farkas[ab] and Vincent M. Rotello *[ab]

Macrophages are plastic cells of the immune system that can be broadly classified as having pro-inflammatory (M1-like) or anti-inflammatory (M2-like) phenotypes. M2-like macrophages are often associated with cancers and can promote cancer growth and create an immune-suppressive tumor microenvironment. Repolarizing macrophages from M2-like to M1-like phenotype provides a crucial strategy for anticancer immunotherapy. Imiquimod is an FDA-approved small molecule that can polarize macrophages by activating toll-like receptor 7/8 (TLR 7/8) located inside lysosomes. However, the non-specific inflammation that results from the drug has limited its systemic application. To overcome this issue, we report the use of gold nanoparticle-based bioorthogonal nanozymes for the conversion of an inactive, imiquimod-based prodrug to an active compound for macrophage re-education from anti- to pro-inflammatory phenotypes. The nanozymes were delivered to macrophages through endocytosis, where they uncaged pro-imiquimod *in situ*. The generation of imiquimod resulted in the expression of pro-inflammatory cytokines. The re-educated M1-like macrophages feature enhanced phagocytosis of cancer cells, leading to efficient macrophage-based tumor cell killing.

Introduction

Macrophages are plastic phagocytes that serve as a first-line defense against pathogens including tumors.[1–3] Macrophage subtypes exist as a complex spectrum with broadly two major phenotypes: classically-activated M1-like macrophages and alternatively-activated M2-like macrophages.[4–6] M1-like macrophages are associated with inflammation by secreting pro-inflammatory cytokines, generating reactive oxygen and nitrogen species, and engulfing antigens to fight viruses, bacteria, or cancers.[7] In contrast, M2-like macrophages reduce inflammation, and promote wound healing and angiogenesis.[5] Studies have revealed, however, that several cancer types can hijack macrophages, which in the tumor environment facilitate proliferation, angiogenesis, and invasion, and provide defense against anticancer therapies.[8–12] These tumor-associated macrophages (TAMs)[13] exist primarily in M2-like phenotype

and can constitute up to 50% of the tumor mass.[14] TAMs provide an immunosuppressive microenvironment surrounding the cancer cells,[15] hampering cancer immunotherapies including immune checkpoint blockades[16] and chimeric antigen receptor (CAR) T cell therapy.[17] Moreover, TAMs can hinder chemotherapy by sacrificing themselves to deplete drugs from cancer cells.[11,18–20] Overall, the M2-like TAMs promote cancer growth and pose an obstacle to multiple efficient cancer therapies.

In contrast, M1-like macrophages display strong antitumor activity. M1-like macrophages can eliminate tumor cells *via* direct phagocytosis and secretion of proinflammatory cytokines that induce the apoptosis of cancer cells.[21] Moreover, M1-like macrophages can also recruit T cells and B cells to the tumor site to initiate the adaptive immune response.[22,23] Therefore, the polarization of TAMs to the M1-like phenotype provides a macrophage-based immunotherapeutic approach to cancer eradication.[24]

Imiquimod is an FDA-approved small molecule toll-like receptor (TLR) agonist that polarizes macrophages to the M1-like phenotype by activating lysosomal TLR7/8.[25–27] Imiquimod is used clinically to treat genital warts[28] and basal cell carcinomas.[29] The therapeutic use of imiquimod requires topical delivery; systemic administration results in non-specific inflammation including cytokine storms.[30] Prodrug strategies

a Department of Chemistry, University of Massachusetts Amherst, 710 N. Pleasant St., Amherst, MA 01003, USA. E-mail: rotello@chem.umass.edu

b Molecular and Cellular Biology Graduate Program, University of Massachusetts Amherst, 230 Stockbridge Road, Amherst, Massachusetts, 01003, USA

† Electronic supplementary information (ESI) available. See DOI: https://doi.org/10.1039/d3sc06431j
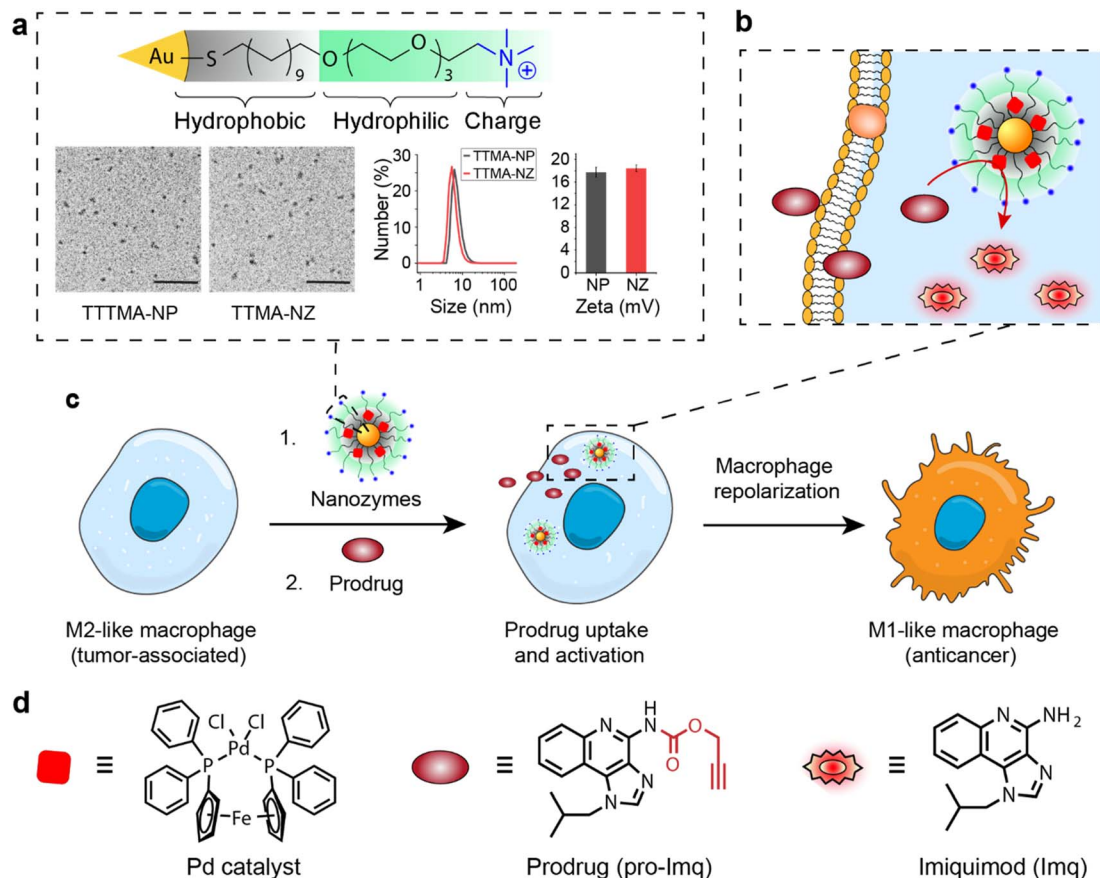
‡ These authors contributed equally.

Fig. 1   (a) Structure, transmission electron microscopy (TEM) imaging, dynamic light scattering (DLS) measurement, and zeta potential of thioalkyl tetra(ethylene glycol) trimethylammonium nanoparticles and nanozymes (**TTMA-NP** and **TTMA-NZ**, respectively). Scale bar = 50 nm. (b) Intracellular activation of the prodrug (**pro-Imq**) by **TTMA-NZ**. (c) Schematic representation of macrophage re-education by nanozyme-mediated imiquimod activation. (d) Structure of the palladium catalyst, **pro-Imq**, and **Imq**.

can minimize off-target effects *via* the use of an inert drug precursor (prodrug), which is converted into the active entity following exposure to either an exogenous or endogenous stimulus.[31–33] Therefore, converting imiquimod from the inactive precursor can potentially avoid cytokine storms throughout the body. Light,[34] enzymes,[35] and redox potential[36] have been used as stimuli to activate imiquimod prodrugs, however, controlled activation and sustained dosing aspects remain challenging.

Bioorthogonal catalysis *via* transition metal catalysts (TMCs) offers an approach for prodrug activation that employs chemical reactions inaccessible to natural enzymes.[37–45] The *in situ* activation of prodrugs overcomes the concern of non-specific leakage of the drug through the conventional delivery strategy. Specifically designed catalysts have shown their potential for drug conversion in biomedical applications,[46–51] however, the direct use of TMCs can face challenges such as limited solubility,[52] low stability,[53] and poor biocompatibility[54] in biological environments. Surface-engineered nanomaterials can solubilize TMCs and protect them from deactivation, providing a modular system for catalysts.[55–58] The loading of TMCs into nanomaterials can be used to fabricate bioorthogonal nanozymes with high catalytic activity for the sustained generation of therapeutics for anticancer,[59–69] antimicrobial,[70–75] and anti-inflammatory treatments.[76]

We report here the use of bioorthogonal nanozymes to re-educate tumor-associated macrophages to pro-inflammatory phenotypes through the intracellular uncaging of an imiquimod prodrug. The encapsulation of palladium catalysts into the monolayer of gold nanoparticles yields bioorthogonal nanozymes and avoids non-specific immunogenicity resulting from the hydrophobic catalysts. Significantly, nanozymes are internalized by macrophages *via* endocytosis, and subsequently activate imiquimod intracellularly, in proximity to the lysosomal TLR7/8 receptors (Fig. 1). The *in situ* generation of imiquimod facilitates macrophage re-education from an M2-like to the M1-like phenotype, evidenced by significant upregulation of inflammatory biomarkers, resulting in enhanced phagocytosis of cancer cells. M1-like macrophages polarized by this nanozyme-based strategy possess efficient anticancer activity and provide a biocompatible strategy for potential cancer immunotherapy use.

Results and discussion

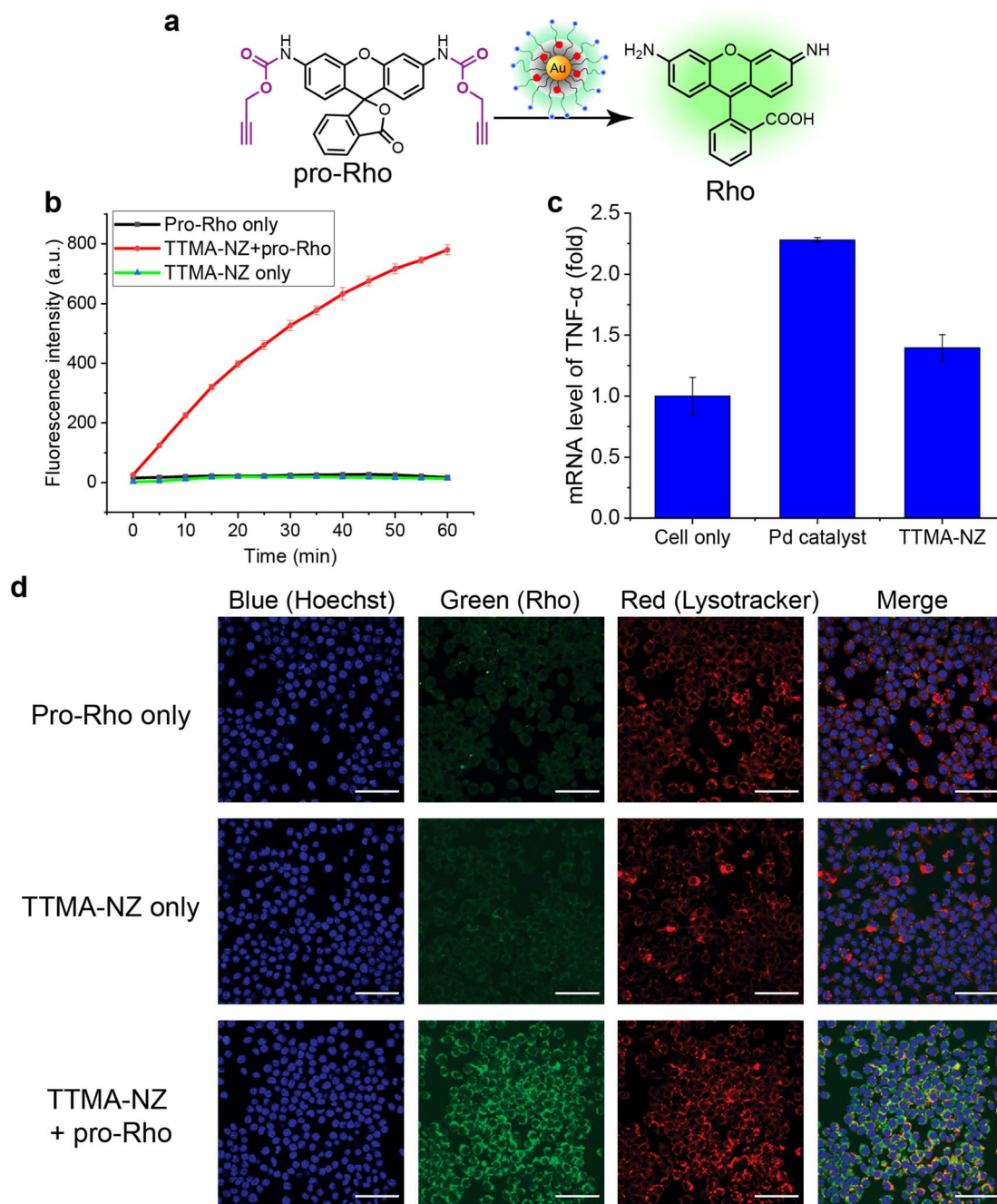The bioorthogonal nanozyme was comprised of palladium catalysts and 2 nm thioalkyl tetra(ethylene glycol)

Fig. 2 (a) **pro-Rho** activation by 400 nM **TTMA-NZ**. (b) Kinetic study of **pro-Rho** activation by **TTMA-NZ** in phosphate-buffered saline (PBS) solution at 37 °C. (c) Quantification of TNF-α mRNA levels following 24 h treatment with free catalysts and **TTMA-NZ** using qRT-PCR. For (b and c), data shown is the average of three replicates; error bars represent standard deviation. (d) Confocal images of RAW 264.7 cells incubated with nanozymes followed by incubation with **pro-Rho** for 24 h and controls. Nuclei were stained by using Hoechst 33342, and lysosomes were stained with deep red Lysotracker. Scale bar = 50 μm. The colocalization of green and red fluorescence indicates the lysosomal activation of the substrate by **TTMA-NZ**.

trimethylammonium ligand (**TTMA**)-functionalized gold nanoparticles (**TTMA-NP**). The **TTMA** ligand consisted of three parts: an aliphatic chain to stabilize the nanoparticle and encapsulate catalysts, an oligo ethylene glycol spacer to enhance water solubility and avoid serum protein denaturation,[56,77,78] and a cationic charge to facilitate efficient endocytosis. The **TTMA** nanozyme (**TTMA-NZ**) was then generated by encapsulating

Pd(dppf)Cl$_2$ catalysts ([1,1′-bis(diphenylphosphino)ferrocene] dichloropalladium(II)) into the nanoparticle through nanoprecipitation. The hydrophobicity of the ligands kept the palladium catalysts inside the hydrophobic monolayer of nanoparticles for a prolonged period.[79] Briefly, Pd catalysts were dissolved in the mixture of acetone and tetrahydrofuran and added dropwise into the nanoparticle solution in water. The
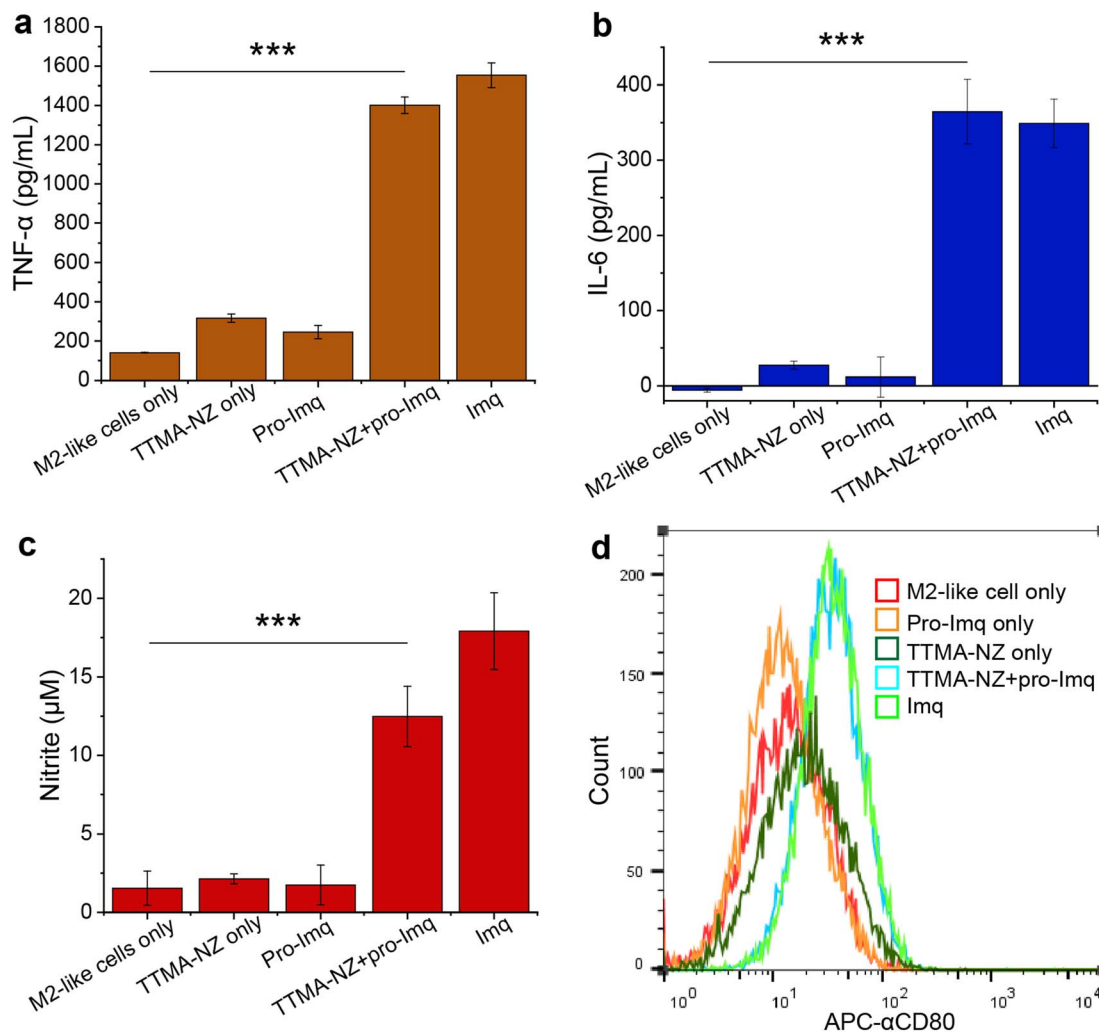
Fig. 3   Re-education of M2-like RAW 264.7 cells by nanozyme-mediated **pro-Imq** activation. Cells were treated with 400 nM nanozymes for 24 h, followed by the addition of 10 μM **pro-Imq** for another 24 h. **Imq** (2 μM) was used as a positive control. Quantification of expression of (a) TNF-α and (b) IL-6 of RAW 264.7 macrophages using enzyme-linked immunosorbent assay (ELISA). (c) Nitrite expression in RAW 264.7 macrophages determined by Griess assay. (d) The expression of M1-related surface marker CD80 tested by flow cytometry using APC-labeled CD80 antibody (APC-αCD80). M2-like RAW 264.7 macrophages treated with nanozymes and **pro-Imq** expressed significantly higher levels of pro-inflammatory biomarkers, showing the re-education of the macrophages to the M1-like phenotype. Data shown is the average of three biological replicates and error bars represent the standard deviation. Statistical significance was determined by a two-tailed Student's t-test. ***: $p < 0.001$.

mixture was applied to a molecular cut-off filter and washed with water to remove excess catalysts to obtain nanozymes. The resulting nanozyme maintained a similar size and surface charge compared to **TTMA-NP** after formulation, as indicated by transmission electron microscopy (TEM), dynamic light scattering (DLS), and zeta potential (Fig. 1a). Inductively coupled plasma mass spectrometry (ICP-MS: ^{106}Pd and ^{197}Au) verified the presence of ∼29 Pd molecules per nanozyme (Table S1†).

The catalytic activity of nanozymes was evaluated through the activation of a caged fluorophore both in solution and in cell culture. The caged fluorophore was prepared by reacting Rhodamine 110 (**Rho**) with propargyl chloroformate to obtain the non-fluorescent precursor (**pro-Rho**).[80] **TTMA-NZ** removes the propargyl groups, resulting in the generation of fluorescent **Rho** (Fig. 2a). The green fluorescence signal increased

significantly after adding nanozymes and **pro-Rho** (Fig. 2b), indicating the decent catalytic activity of nanozymes. The rate (∼2 nM min^{-1}) was calculated by the calibration curve of **Rho** (Fig. S1†). This activity was further probed in RAW 264.7 murine macrophage cells (M0 macrophages) through intracellular imaging. A cytotoxicity study was first performed to optimize the working concentration of nanozymes. Results showed that 400 nM **TTMA-NZ** started to have slight toxicity after 48 h treatment, 50 nM nanozyme, however, started to be toxic after 72 h treatment (Fig. S2†). Non-specific immunogenicity of the agents toward macrophages was then determined by evaluating the mRNA expression of the pro-inflammatory biomarker tumor necrosis factor-α (TNF-α) following 24 h treatment with **TTMA-NZ** (400 nM, containing 11.6 μM Pd catalysts) or the same amount of free catalysts (11.6 μM) using quantitative real-time
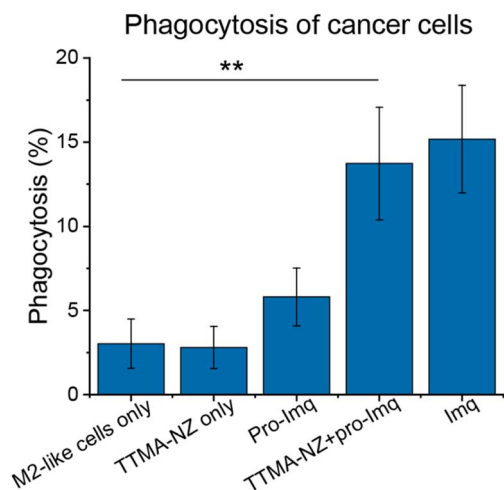
Phagocytosis of cancer cells

Fig. 4 Phagocytosis percentage of M2-like RAW 264.7 macrophages against U2OS cells determined by flow cytometry (Fig. S10†). Cells were treated with 400 nM nanozymes for 24 h followed by the addition of 10 μM pro-Imq for another 24 h. Imq (2 μM) was used as a positive control. Nanozyme-based strategy resulted in elevated phagocytosis by ~4-fold compared to untreated controls. Data shows the average of three biological replicates and error bars represent the standard deviation. Statistical significance was determined by a two-tailed Student's t-test. **: $0.01 > p > 0.001$.

polymerase chain reaction (qRT-PCR). Compared to the free catalysts, nanozymes are much less immunogenic, presumably due to the shielding of the hydrophobic catalysts from the environment (Fig. 2c). **TTMA-NZ** was then used for **pro-Rho** activation *in vitro*. Confocal microscopy showed the generation of green fluorescence inside the macrophages that were treated with nanozymes and **pro-Rho** (Fig. 2d). Considering **pro-Rho** cannot be activated by cellular components, fluorogenesis indicates that nanozymes retain significant activity inside the living cells. Significantly, the green fluorescence co-localized with red fluorescence from the Lysotracker, mirroring the *in situ* intracellular uncaging of substrates inside the lysosomes.

Encouraged by the results obtained from cell imaging, we applied the same caging strategy to generate a prodrug of the pro-inflammatory drug imiquimod (**pro-Imq**; synthesis and characterization in Fig. S3–S5†). **pro-Imq** was obtained by blocking the imiquimod (**Imq**) pharmacophore with a propargyloxycarbonyl group. Compared to **Imq**, **pro-Imq** resulted in a more than 50-fold lower expression of the pro-inflammatory cytokine TNF-α (Fig. S6a†) and only 10 μM **pro-Imq** started to have slight toxicity after 72 h treatment (Fig. S6†). Even though immortalized macrophages mimic the main phenotypical and metabolic features of their primary cell counterparts, they still differ in multiple aspects.[81] We therefore, also tested the cytotoxicity of **TTMA-NZ** and **pro-Imq** on primary bone marrow-derived macrophages (BMDMs) isolated from C57/B6J mice (Fig. S7†), which demonstrated that **TTMA-NZ** and **pro-Imq** showed even lower toxicity toward BMDMs compared to RAW 264.7 cells. Based on the cytotoxicity results, 400 nM **TTMA-NZ**, 10 μM **pro-Imq** and 2 μM **Imq** were used for the following studies.

We next investigated macrophage re-polarization through intracellular uncaging of the **pro-Imq** using nanozymes. M2-like

macrophages were induced by incubating RAW 264.7 cells with interleukin-4 (lL-4) for 24 h. The M2-polarized RAW 264.7 macrophages were then incubated with nanozymes for 24 h, followed by washing with PBS four times to remove the non-internalized nanozymes. **pro-Imq** was then added to the cells. After 24 h, the supernatant was collected for analysis. The **pro-Imq** and **Imq** alone were used as negative and positive controls, respectively. The re-polarization of M2-like macrophages to M1-like macrophages was investigated through analysis of the expression of pro-inflammatory cytokines (TNF-α and interleukin-6 (IL-6)), and nitrite production. Nanozyme and **pro-Imq** treated RAW 264.7 macrophages expressed significantly higher levels of all three proinflammatory signaling molecules (Fig. 3), comparable to the positive controls. Negative controls (nanozyme and **pro-Imq**, independently) did not show elevated expression of pro-inflammatory cytokines or nitrite levels. M1-like polarization was further assessed by analyzing the expression of the M1-like macrophage-related surface marker CD80. CD80 serves as a co-stimulatory molecule for T cell activation that initiates cell-based immunotherapy.[82] RAW 264.7 macrophages treated with nanozymes and **pro-Imq** showed a two-fold greater expression of CD80 receptors *versus* negative control groups, as determined by flow cytometry (Fig. 3d). Together, *in situ* uncaging of **pro-Imq** by nanozymes results in the efficient polarization of RAW 264.7 macrophages to M1-like macrophages. In addition, we determined the TNF-α and IL-6 expression of IL-4-induced M2-like BMDMs after treatment with nanozyme and **pro-Imq** (Fig. S8†). The significantly increased levels of TNF-α and IL-6 indicated that nanozymes uncaging **pro-Imq** *in situ* can also induce efficient M2-like to M1-like repolarization of primary macrophages, further demonstrating the immunotherapeutic potential of our system.

A key aspect of macrophage-mediated anticancer activity is their engulfment of cancer cells *via* phagocytosis;[83–85] M2-like macrophages repolarized to the M1-like phenotype have enhanced phagocytosis.[86] We tested the phagocytic ability of M1-like macrophages re-polarized by the nanozyme-based treatment against green-fluorescent protein-expressing osteosarcoma U2OS cancer cells (GFP-U2OS cells). The cytotoxicity of **Imq** itself toward GFP-U2OS cells was first determined (Fig. S9†), with 2 μM **Imq** exhibiting no toxicity after up to 72 h treatment. For phagocytosis studies, M2-like RAW 264.7 macrophages were pre-treated with nanozymes and **pro-Imq** subsequently. Afterward, the macrophages were harvested and labeled by phycoerythrin (PE)-conjugated F4/80 antibody. The cells were then washed and incubated with GFP-U2OS cells for 4 h at 37 °C. Phagocytosis was evaluated by tracking the red PE channel and green FITC channel using flow cytometry. RAW 264.7 macrophages treated with NZ and **pro-Imq** showed a 4-fold increase in phagocytosis of U2OS cells compared to the non-treated controls, reaching the same level as the positive control (Fig. 4 and S10†). This result reflects the efficient recognition and engulfment of cancer cells by the re-educated macrophages using nanozymes.

The anti-cancer potential of nanozyme re-educated macrophages was further evaluated through a co-culture model. M2-like RAW 264.7 macrophages were seeded with GFP-U2OS
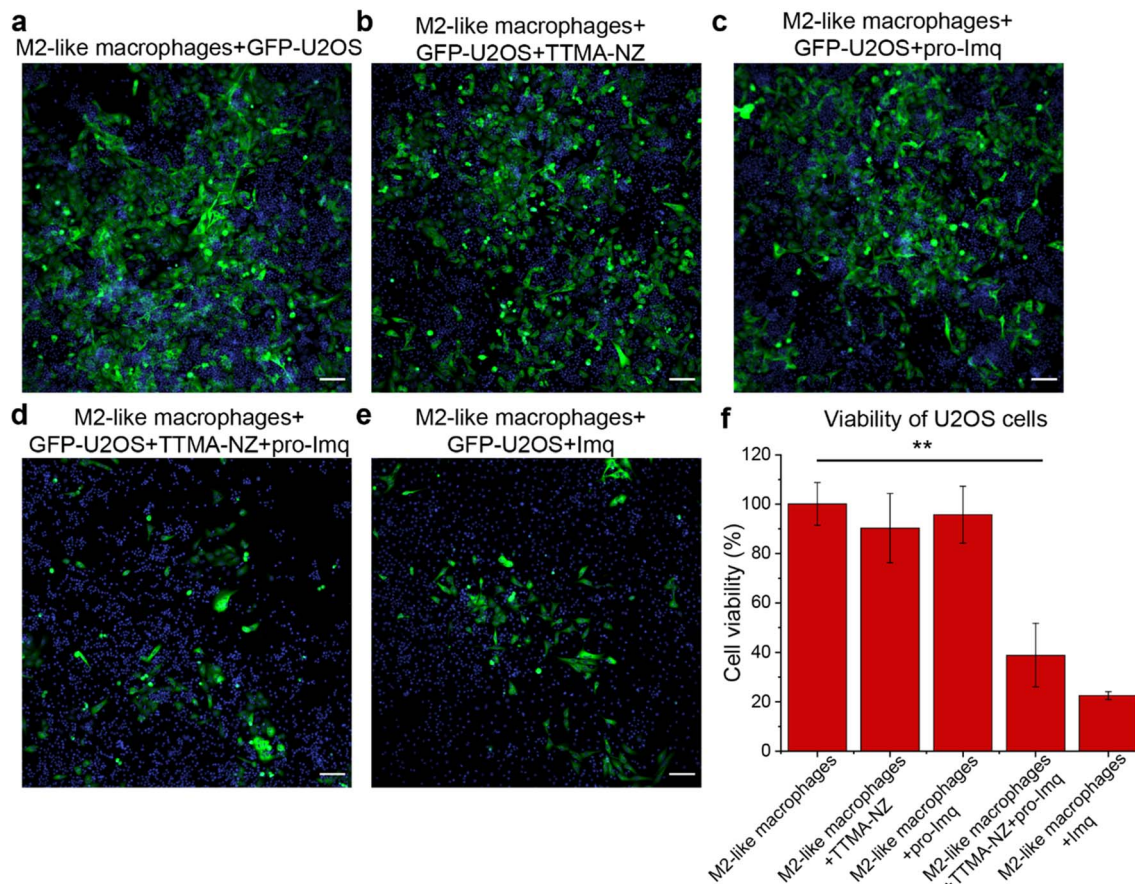
Fig. 5 Confocal imaging of M2-like RAW 264.7 macrophages and GFP-U2OS cells (a) without further treatment, and with M2 macrophages treated by (b) pro-Imq, (c) Imq, (d) TTMA-NZ, and (e) TTMA-NZ + pro-Imq subsequently. Where applicable, cells were treated with nanozymes (400 nM) and pro-Imq (10 μM). Imq (2 μM) was used as the positive control. The nucleus was stained by Hoechst 33342. Scale bar = 100 μm. (f) Viability of cancer cells. The result was determined by tracking the intensity of green fluorescence. Data shows the average of triplicates and error bars represent the standard deviation. Statistical significance was determined by a two-tailed Student's t-test. **: $0.01 > p > 0.001$.

cells in confocal microscopy dishes followed by sequential treatment with nanozymes, **pro-Imq** and indicated controls. The cells were then incubated for 24 h and imaged using confocal microscopy. GFP fluorescence was used as a surrogate readout for the viability of the cancer cells. Diminished levels of green fluorescence were observed for cells treated with nanozymes and **pro-Imq**, and **Imq** alone, which can be attributed to cancer cell death and/or inhibition of proliferation. As expected, nanozyme alone or **pro-Imq** alone showed no appreciable effects on the cancer cells (Fig. 5).

Conclusion

In summary, we report the polarization of tumor-associated macrophages to an anticancer phenotype by *in situ* TLR 7/8 agonist activation using bioorthogonal nanozymes. The nanozymes were located inside endosomes/lysosomes following uptake by macrophages and provided on-target uncaging of an imiquimod prodrug. This uncaged imiquimod re-educated anti-inflammatory M2-like macrophages to anticancer M1-like cells. The re-educated M1-like macrophages possessed enhanced phagocytosis capabilities and resulted in diminished levels of

cancer cells *versus* controls. This study demonstrates the polarization of macrophages for anticancer applications by harnessing the endocytosis of bioorthogonal nanozymes combined with the administration of an inert prodrug. The nanozymes act as a localized "drug factory", enabling the innate immune system to fight cancer with minimized side effects. Translation to *in vivo* application will take advantage of the prodrug design, allowing pro-imiquimod to be injected intravenously due to the reduced likelihood of non-specific inflammation. The re-polarization of M2-like TAMs for cancer immunotherapy can also be coupled with *in situ* chemotherapy to provide immuno-chemotherapy for enhanced therapeutic effects.

Data availability

The data supporting the findings of this study are available within the article and in the ESI.†

Author contributions

Xianzhi Zhang: conceptualization, methodology, investigation, formal analysis, project administration, data curation, writing-original draft, visualization, writing-review & editing.

Conflicts of interest

There are no conflicts to declare.

Acknowledgements

References

1 Y. Liu, J. Hardie, X. Zhang and V. M. Rotello, *Semin. Immunol.*, 2017, **34**, 25–32.

2 D. C. Luther, R. Huang, T. Jeon, X. Zhang, Y. W. Lee, H. Nagaraj and V. M. Rotello, *Adv. Drug Delivery Rev.*, 2020, **156**, 188–213.

3 P. J. Murray and T. A. Wynn, *Nat. Rev. Immunol.*, 2011, **11**, 723–737.

4 P. J. Murray, J. E. Allen, S. K. Biswas, E. A. Fisher, D. W. Gilroy, S. Goerdt, S. Gordon, J. A. Hamilton, L. B. Ivashkiv, T. Lawrence, M. Locati, A. Mantovani, F. O. Martinez, J.-L. Mege, D. M. Mosser, G. Natoli, J. P. Saeij, J. L. Schultze, K. A. Shirey, A. Sica, J. Suttles, I. Udalova, J. A. van Ginderachter, S. N. Vogeln and T. A. Wynn, *Immunity*, 2014, **41**, 14–20.

5 D. M. Mosser and J. P. Edwards, *Nat. Rev. Immunol.*, 2008, **8**, 958–969.

6 T. A. Wynn, A. Chawla and J. W. Pollard, *Nature*, 2013, **496**, 445–455.

7 G. A. Duque and A. Descoteaux, *Front. Immunol.*, 2014, **5**, 491.

8 A. Mantovani, P. Allavena, F. Marchesi and C. Garlanda, *Nat. Rev. Drug Discovery*, 2022, **21**, 799–820.

9 E. Y. Lin and J. W. Pollard, *Cancer Res.*, 2007, **67**, 5064–5066.

10 A. Mantovani, S. Sozzani, M. Locati, P. Allavena and A. Sica, *Trends Immunol.*, 2002, **23**, 549–555.

11 A. Mantovani, B. Bottazzi, F. Colotta, S. Sozzani and L. Ruco, *Immunol. Today*, 1992, **13**, 265–270.

12 R. A. Franklin, W. Liao, A. Sarkar, M. V. Kim, M. R. Bivona, K. Liu, E. G. Pamer and M. O. Li, *Science*, 2014, **344**, 921–925.

13 R. Noy and J. W. Pollard, *Immunity*, 2014, **41**, 49–61.

14 I. Larionova, G. Tuguzbaeva, A. Ponomaryova, M. Stakheyeva, N. Cherdyntseva, V. Pavlov, E. Choinzonov and J. Kzhyshkowska, *Front. Oncol.*, 2020, **10**, 1–34.

15 P. Pathria, T. L. Louis and J. A. Varner, *Trends Immunol.*, 2019, **40**, 310–327.

16 S. P. Arlauckas, C. S. Garris, R. H. Kohler, M. Kitaoka, M. F. Cuccarese, K. S. Yang, M. A. Miller, J. C. Carlson, G. J. Freeman, R. M. Anthony, R. Weissleder and M. J. Pittet, *Sci. Transl. Med.*, 2017, **9**, eaal3604.

17 A. Rodriguez-Garcia, R. C. Lynn, M. Poussin, M. A. Eiva, L. C. Shaw, R. S. O'Connor, N. G. Minutolo, V. Casado-Medrano, G. Lopez, T. Matsuyama and D. J. Powell, *Nat. Commun.*, 2021, **12**, 1–17.

18 O. C. Olson, H. Kim, D. F. Quail, E. A. Foley and J. A. Joyce, *Cell Rep.*, 2017, **19**, 101–113.

19 Q. Dai, S. Wilhelm, D. Ding, A. M. Syed, S. Sindhwani, Y. Zhang, Y. Y. Chen, P. Macmillan and W. C. W. Chan, *ACS Nano*, 2018, **12**, 8423–8435.

20 M. De Palma and C. E. Lewis, *Cancer Cell*, 2013, **23**, 277–286.

21 M. Xiao, J. He, L. Yin, X. Chen, X. Zu and Y. Shen, *Front. Immunol.*, 2021, **12**, 799428.

22 D. G. DeNardo and B. Ruffell, *Nat. Rev. Immunol.*, 2019, **19**, 369–382.

23 Q. Jin, Z. Liu and Q. Chen, *J. Controlled Release*, 2021, **329**, 882–893.

24 J. Liu, Q. Chen, L. Feng and Z. Liu, *Nano Today*, 2018, **21**, 55–73.

25 C. Zhao, X. Pang, Z. Yang, S. Wang, H. Deng and X. Chen, *J. Controlled Release*, 2022, **341**, 272–284.

26 Y. Xia, L. Rao, H. Yao, Z. Wang, P. Ning and X. Chen, *Adv. Mater.*, 2020, **32**, 1–20.

27 S. Bhagchandani, J. A. Johnson and D. J. Irvine, *Adv. Drug Delivery Rev.*, 2021, **175**, 113803.

28 R. Moore, J. E. Edwards, J. Hopwood and D. Hicks, *BMC Infect. Dis.*, 2001, **1**, e3.

29 R. I. Ceilley and J. Q. Del Rosso, *Int. J. Dermatol.*, 2006, **45**, 489–498.

30 P. Kamath, E. Darwin, H. Arora and K. Nouri, *Clin. Drug Invest.*, 2018, **38**, 883–899.

31 J. Rautio, H. Kumpulainen, T. Heimbach, R. Oliyai, D. Oh, T. Järvinen and J. Savolainen, *Nat. Rev. Drug Discovery*, 2008, **7**, 255–270.

32 J. Rautio, N. A. Meanwell, L. Di and M. J. Hageman, *Nat. Rev. Drug Discovery*, 2018, **17**, 559–587.

33 R. Walther, J. Rautio and A. N. Zelikin, *Adv. Drug Delivery Rev.*, 2017, **118**, 65–77.

34 K. A. Ryu, L. Stutts, J. K. Tom, R. J. Mancini and A. P. Esser-Kahn, *J. Am. Chem. Soc.*, 2014, **136**, 10823–10825.

35 J. D. Hantho, T. A. Strayer, A. E. Nielsen and R. J. Mancini, *ChemMedChem*, 2016, **11**, 2496–2500.

36 H. Lei, J. H. Kim, S. Son, L. Chen, Z. Pei, Y. Yang, Z. Liu, L. Cheng and J. S. Kim, *ACS Nano*, 2022, **16**, 10979–10993.

37 T. Liang, Z. Chen, H. Li and Z. Gu, *Trends Chem.*, 2022, **4**, 157–168.

38 X. Zhang, R. Huang, S. Gopalakrishnan, R. Cao-milán and V. M. Rotello, *Trends Chem.*, 2019, **1**, 90–98.

39 Y. Huang, J. Ren and X. Qu, *Chem. Rev.*, 2019, **119**, 4357–4412.

40 J. Wu, X. Wang, Q. Wang, Z. Lou, S. Li, Y. Zhu, L. Qin and H. Wei, *Chem. Soc. Rev.*, 2019, **48**, 1004–1076.

41 M. O. N. van de L'Isle, M. C. Ortega-Liebana and A. Unciti-Broceta, *Curr. Opin. Chem. Biol.*, 2021, **61**, 32–42.

42 D. P. Nguyen, H. T. H. Nguyen and L. H. Do, *ACS Catal.*, 2021, **11**, 5148–5165.

43 M. Martínez-calvo and J. L. Mascareñas, *Coord. Chem. Rev.*, 2018, **359**, 57–79.

44 Y. Liu and Y. Bai, *ACS Appl. Bio Mater.*, 2020, **3**, 4717–4746.

45 B. Lozhkin and T. R. Ward, *Bioorg. Med. Chem.*, 2021, **45**, 116310.

46 S. Bose, A. H. Ngo and L. H. Do, *J. Am. Chem. Soc.*, 2017, **139**, 8792–8795.

47 T. Völker, F. Dempwolff, P. L. Graumann and E. Meggers, *Angew. Chem., Int. Ed.*, 2014, **53**, 10536–10540.

48 T. Völker and E. Meggers, *Chembiochem*, 2017, **18**, 1083–1086.

49 M. Tomás-Gamasa, M. Martínez-Calvo, J. R. Couceiro and J. L. Mascareñas, *Nat. Commun.*, 2016, **7**, 12538.

50 M. Martínez-Calvo, J. R. Couceiro, P. Destito, J. Rodríguez, J. Mosquera and J. L. Mascareñas, *ACS Catal.*, 2018, **8**, 6055–6061.

51 C. Vidal, M. Tomás-Gamasa, A. Gutiérrez-González and J. L. Mascareñas, *J. Am. Chem. Soc.*, 2019, **141**, 5125–5129.

52 G. Y. Tonga, Y. Jeong, B. Duncan, T. Mizuhara, R. Mout, R. Das, S. T. Kim, Y. C. Yeh, B. Yan, S. Hou and V. M. Rotello, *Nat. Chem.*, 2015, **7**, 597–603.

53 X. Zhang, S. Fedeli, S. Gopalakrishnan, R. Huang, A. Gupta, D. C. Luther and V. M. Rotello, *ChemBioChem*, 2020, **21**, 2759–2763.

54 Y. Liu, S. Pujals, P. J. M. Stals, T. Paulöhrl, S. I. Presolski, E. W. Meijer, L. Albertazzi and A. R. A. Palmans, *J. Am. Chem. Soc.*, 2018, **140**, 3423–3433.

55 X. Zhang, R. F. Landis, P. Keshri, R. Cao-Milán, D. C. Luther, S. Gopalakrishnan, Y. Liu, R. Huang, G. Li, M. Malassiné, I. Uddin, B. Rondon and V. M. Rotello, *Adv. Healthcare Mater.*, 2020, **10**, 2001627.

56 X. Zhang, Y. Liu, S. Gopalakrishnan, L. Castellanos-Garcia, G. Li, M. Malassiné, I. Uddin, R. Huang, D. Luther, R. Vachet and V. Rotello, *ACS Nano*, 2020, **14**, 4767–4773.

57 S. Fedeli, J. Im, S. Gopalakrishnan, J. L. Elia, A. Gupta, D. Kim and V. M. Rotello, *Chem. Soc. Rev.*, 2021, **50**, 13467–13480.

58 W. Wang, X. Zhang, R. Huang, C. M. Hirschbiegel, H. Wang, Y. Ding and V. M. Rotello, *Adv. Drug Delivery Rev.*, 2021, **176**, 113893.

59 X. Zhang, S. Lin, R. Huang, A. Gupta, S. Fedeli, R. Cao-Milán, D. C. Luther, Y. Liu, M. Jiang, G. Li, B. Rondon, H. Wei and V. M. Rotello, *J. Am. Chem. Soc.*, 2022, **144**, 12893–12900.

60 M. Sancho-albero, B. Rubio-ruiz, A. M. Pérez-lópez, V. Sebastián, P. Martín-duque, M. Arruebo, J. Santamaría and A. Unciti-broceta, *Nat. Catal.*, 2019, **2**, 864–872.

61 S. Eda, I. Nasibullin, K. Vong, N. Kudo, M. Yoshida, A. Kurbangalieva and K. Tanaka, *Nat. Catal.*, 2019, **2**, 780–792.

62 C. Adam, T. L. Bray, A. M. Pérez-López, E. H. Tan, B. Rubio-Ruiz, D. J. Baillache, D. R. Houston, M. J. Salji, H. Y. Leung and A. Unciti-Broceta, *J. Med. Chem.*, 2022, **65**, 552–561.

63 R. Das, J. Hardie, B. P. Joshi, X. Zhang, A. Gupta, D. C. Luther, S. Fedeli, M. E. Farkas and V. M. Rotello, *JACS Au*, 2022, **2**, 1679–1685.

64 Z. Chen, H. Li, Y. Bian, Z. Wang, G. Chen, X. Zhang, Y. Miao, D. Wen, J. Wang, G. Wan, Y. Zeng, P. Abdou, J. Fang, S. Li, C.-J. Sun and Z. Gu, *Nat. Nanotechnol.*, 2021, **16**, 933–941.

65 M. A. Miller, B. Askevold, H. Mikula, R. H. Kohler, D. Pirovich and R. Weissleder, *Nat. Commun.*, 2017, **8**, 15906.

66 M. A. Miller, H. Mikula, G. Luthria, R. Li, S. Kronister, M. Prytyskach, R. H. Kohler, T. Mitchison and R. Weissleder, *ACS Nano*, 2018, **12**, 12814–12826.

67 Y. You, Q. Deng, Y. Wang, Y. Sang, G. Li, F. Pu, J. Ren and X. Qu, *Nat. Commun.*, 2022, **13**, 1459.

68 Y. Wei, S. Wu, Z. Liu, J. Niu, Y. Zhou, J. Ren and X. Qu, *Mater. Today*, 2022, **56**, 16–28.

69 Y. You, H. Liu, J. Zhu, Y. Wang, F. Pu, J. Ren and X. Qu, *Chem. Sci.*, 2022, **13**, 7829–7836.

70 J. Hardie, J. M. Makabenta, A. Gupta, R. Huang, R. Cao-Milán, R. Goswami, X. Zhang, P. Abdulpurkar, M. E. Farkas and V. M. Rotello, *Mater. Horiz.*, 2022, **9**, 1489–1494.

71 R. Huang, C. Li, R. Cao-milan, L. D. He, J. M. Makabenta, X. Zhang, E. Yu and V. M. Rotello, *J. Am. Chem. Soc.*, 2020, **142**, 10723–10729.

72 R. Cao-milan, S. Gopalakrishnan, L. D. He, R. Huang, L. Wang, L. Castellanos, D. C. Luther, R. F. Landis, J. M. V Makabenta, C. Li, X. Zhang, F. Scaletti, R. W. Vachet and V. M. Rotello, *Chem*, 2020, **6**, 1–12.

73 A. Gupta, R. Das, J. M. Makabenta, A. Gupta, X. Zhang, T. Jeon, R. Huang, Y. Liu, S. Gopalakrishnan, R. C. Milán and V. M. Rotello, *Mater. Horiz.*, 2021, **8**, 3424–3431.

74 J. Niu, L. Wang, T. Cui, Z. Wang, C. Zhao, J. Ren and X. Qu, *ACS Nano*, 2021, **15**, 15841–15849.

75 J. Niu, C. Zhao, C. Liu, J. Ren and X. Qu, *Chem. Mater.*, 2021, **33**, 8052–8058.

76 Z. Du, C. Liu, H. Song, P. Scott, Z. Liu, J. Ren and X. Qu, *Chem*, 2020, **6**, 2060–2072.

77 S. T. Kim, K. Saha, C. Kim and V. M. Rotello, *Acc. Chem. Res.*, 2013, **46**, 681–691.

78 J. W. E. Worrall, A. Verma, H. Yan and V. M. Rotello, *Chem. Commun.*, 2006, 2338–2340.

79 X. Zhang, Y. Liu, J. Doungchawee, L. J. Castellanos-García, K. N. Sikora, T. Jeon, R. Goswami, S. Fedeli, A. Gupta, R. Huang, C.-M. Hirschbiegel, R. Cao-Milán, P. K. D. Majhi, Y. A. Cicek, L. Liu, D. J. Jerry, R. W. Vachet and V. M. Rotello, *J. Controlled Release*, 2023, **357**, 31–39.

80 R. Huang, C. M. Hirschbiegel, X. Zhang, A. Gupta, S. Fedeli, Y. Xu and V. M. Rotello, *ACS Appl. Mater. Interfaces*, 2022, **14**, 31594–31600.

81 M. Their, M. P. State, I. Spera, S. Ricardo, M. Favia, A. Menga, F. C. Venegas, R. Angioni, F. Munari, M. Lanza, A. Campanella, C. L. Pierri, M. Canton and A. Castegna, *Cancers*, 2021, **13**, 5478.

82 M. Canel, D. Taggart, A. H. Sims, D. W. Lonergan, I. C. Waizenegger and A. Serrels, *Elife*, 2020, **9**, e48092.

83 M. Ray, Y. W. Lee, J. Hardie, R. Mout, G. Yeşilbag Tonga, M. E. Farkas and V. M. Rotello, *Bioconjugate Chem.*, 2018, **29**, 445–450.

84 L. Tian, M. Shao, Y. Gong, T. Wei, Y. Zhu, Y. Chao and Z. Liu, *Bioconjugate Chem.*, 2022, **33**, 343–352.

85 X. Zhou, X. Liu and L. Huang, *Adv. Funct. Mater.*, 2021, **31**, 2006220.

86 J. Hardie, J. A. Mas-Rosario, S. Ha, E. M. Rizzo and M. E. Farkas, *Pharmacol. Res.*, 2019, **148**, 104452.